

Simulations of the Erythrocyte Cytoskeleton at Large Deformation.

I. Microscopic Models

Seng K. Boey, David H. Boal, and Dennis E. Discher

*Department of Physics, Simon Fraser University, Burnaby, British Columbia V5A 1S6, Canada

ABSTRACT Three variations of a polymer chain model for the human erythrocyte cytoskeleton are used in large deformation simulations of microscopic membrane patches. Each model satisfies an experimental observation that the contour length of the spectrin tetramers making up the erythrocyte cytoskeleton is roughly $\sqrt{7}$ times the end-to-end distance of the tetramer in vivo. Up to modest stress, each brushy cytoskeletal network behaves, consistently, like a low-temperature, planar network of Hookean springs, with a model-dependent effective spring constant, k_{eff} , in the range of $20\text{--}40 k_B T/s_o^2$, where T is the temperature and s_o is the force-free spring length. However, several features observed at large deformation distinguish these models from spring networks: 1) Network dimensions do not expand without bound in approaching a critical isotropic tension ($\sqrt{3} k_{\text{eff}}$) that is a characteristic limit of Hookean spring nets. 2) In surface compression, steric interactions among the chain elements prevent a network collapse that is otherwise observed in compression of planar triangulated networks of springs. 3) Under uniaxial surface tension, isotropy of the network disappears only as the network is stretched by more than 50% of its equilibrium dimensions. Also found are definitively non-Hookean regimes in the stress dependence of the elastic moduli. Lastly, determinations of elastic moduli from both fluctuations and stress/strain relations prove to be consistent, implying that consistency should be expected among experimental determinations of these quantities.

INTRODUCTION

The mean diameter of a human erythrocyte is $\sim 8 \mu\text{m}$, yet the cell routinely passes through capillaries with half that diameter or less. The surface shear resistance of the erythrocyte must not be too large, or the cell could not deform easily in a capillary. On the other hand, surface shear resistance must be large enough to maintain the cell's shape and integrity during normal flow in the circulatory system. As the human erythrocyte has no significant intracellular structure, the in-plane elasticity of the plasma membrane likely arises in no small part from the membrane-associated cytoskeleton, a cross-linked brushy polymer network. The protein spectrin is the primary component of the cytoskeletal network: spectrin cross-links very short actin filaments, resulting in junctional nodes that are approximately five- or sixfold coordinated in spectrin.

The in-plane elastic constants of the network—shear and area compression moduli—have been measured at vanishingly small (Zilker et al., 1992; Peterson et al., 1992; Strey et al., 1995) and moderate (Waugh and Evans, 1979; Hochmuth, 1987; Engelhardt and Sackmann, 1988; Discher et al., 1994) stress. The various measurements indicate that the shear and area compression moduli are both less than or on the order of 10^{-5} J/m^2 , which is about the order of magni-

tude one would expect from the density of junction vertices in the cytoskeleton. That is, both a two-dimensional ideal gas and a triangulated network of loose chains have an area compression modulus K_A of $\beta K_A A_j \approx 1$, where β is the inverse temperature ($1/k_B T$) and A_j is the area per particle or per network node (i.e., junction). Explicitly, given a node density of $2 \times 10^{14} \text{ m}^{-2}$ of the cytoskeleton junction vertices, such two-dimensional systems would have an area compression modulus of $\sim 10^{-6} \text{ J/m}^2$ (or $1 \text{ pN}/\mu\text{m}$) at room temperature (for which $\beta^{-1} = 4.0 \times 10^{-21} \text{ J}$).

However, these order of magnitude estimates and the two most commonly quoted measurements of the elastic moduli do not agree in detail. In recent flicker experiments (Zilker et al., 1992; Peterson et al., 1992; Strey et al., 1995), long wavelength fluctuations of the erythrocyte shape suggest that the shear modulus is consistent with zero. In contrast, micropipette aspiration experiments (Waugh and Evans, 1979; Hochmuth, 1987; Discher et al., 1994), which involve large deformations of an erythrocyte, yield an apparent shear modulus of $6\text{--}9 \times 10^{-6} \text{ J/m}^2$. The difference between these measurements could arise from several effects, including the following:

The elastic moduli of two-dimensional triangulated networks are known to be stress-dependent (Boal et al., 1993).

The elastic moduli of two-dimensional polymerized networks fluctuating in three dimensions are known to be wavelength-dependent (Nelson and Peliti, 1987; Aronovitz and Lubensky, 1988; David and Gitter, 1988; Le Doussal and Radzihovsky, 1992).

In this paper, we investigate the stress dependence of model networks of the erythrocyte cytoskeleton in deformation, particularly large deformation.

In an earlier publication (Boal, 1994), a computational model was developed for the cytoskeleton, using a network

Received for publication 28 January 1998 and in final form 14 May 1998.

Address reprint requests to Dr. David H. Boal, Dept. of Physics, Simon Fraser University, Burnaby, BC V5A 1S6 Canada. Tel.: 604-291-5765; Fax: 604-291-3592; E-mail: boal@sfu.ca.

Dr. Boey's current address is Inex Pharmaceuticals, Burnaby, BC V5J 5J8 Canada.

Dr. Discher's current address is Towne Building 112, University of Pennsylvania, 220 S. 33d St., Philadelphia, PA 19104-6315 USA.

© 1998 by the Biophysical Society

0006-3495/98/09/1573/11 \$2.00

of polymer chains attached to each other at sixfold junctions, and attached to a flat computational bilayer at the chain midpoints (see Fig. 1 *a*). The primary motivation for the microscopic structure of this model is the experimental observation that in fully spread, negatively stained skeletons, the contour length of the spectrin tetramer that makes up the erythrocyte cytoskeleton is about $\sqrt{7}$ times the end-to-end distance in vivo (Byers and Branton, 1985; Liu et al., 1987; see also Steck, 1989). However, it has been suggested that the imaging technique used in these experiments may disrupt in vivo associations that may be present both within and between spectrin tetramers, leading to an artificially high estimate of the effective contour length in vivo (Ursitti and Wade, 1993).

Sample configurations of a polymer-chain network under stress are shown in Fig. 1, where Fig. 1 *a* shows a network under tension, and Fig. 1 *b* shows the same network under compression. Note in Fig. 1 *a* that the chain midpoints can be seen, from the gray scale, as residing closest to the $z = 0$ plane. At zero stress, a state between the two illustrated, the chains are significantly convoluted, reflecting the fact that the area per junction vertex is fixed at a small fraction of its stretched or contour value. The elastic properties of the model network at zero stress agree in part with the observations obtained by micromechanical manipulation of the erythrocyte. However, it is important to understand the properties of the model network away from the small stress regime, both because some of the experimental measurements were made under such conditions, and because the erythrocyte is placed under significant stress in the circulatory system.

In this paper, we determine the stress dependence of the geometry and elasticity of the polymer-chain model, particularly the network area and two-dimensional elastic properties. The stress dependence of out-of-plane properties, such as network thickness and bulk modulus, are also re-

ported. At this time, machine limitations prevent us from examining polymer chain systems whose equivalent physical dimension exceeds $\sim 0.3 \mu\text{m}$ to the side, which is far smaller than a typical erythrocyte. Hence, in the second of this pair of papers (Discher et al., 1998, referred to as paper II hereafter) we coarse-grain the present models by constructing effective representations in which entire chains are replaced with two- and three-body potentials. With this representation, a complete erythrocyte with 10^4 or so junction complexes can be simulated on inexpensive workstations. Results from these “whole cell” simulations, and comparisons with experiment, are elaborated in paper II.

It was assumed in our first investigation of the polymer-chain model that the cytoskeleton of a normal mature erythrocyte is not under stress (which we refer to in this paper as the stress-free model). Here we examine two other situations that may be relevant to the erythrocyte:

1. The cytoskeleton may be under compression in a normal erythrocyte. For example, a “prestress” of the cytoskeleton could arise from the preferential loss of bilayer (Discher et al., 1994) as membrane area is lost in erythrocyte maturation (Mohandas and Groner, 1989). The concept of a prestress imposed by the bilayer on the cytoskeleton has been explicitly discussed by Kozlov and Markin (1995) and implicitly employed by Mohandas and Evans (1994) in the proposal of constitutive equations for membrane tensions (see equation 7 in Mohandas and Evans, 1994). Recent and careful optical measurements of the area of isolated cytoskeletons (Svoboda et al., 1992) show the area to be smaller than the intact red cell's, but not nearly so small as expected (see Boal, 1994) in the absence of the constraining bilayer. Last, recent theoretical arguments (Goulian et al., 1993) show that bilayer thermal fluctuations can lead to attraction between integral membrane proteins, including those attached to an underlying cytoskeleton; this would be equivalent to imposing a compressive force on the cytoskeleton.

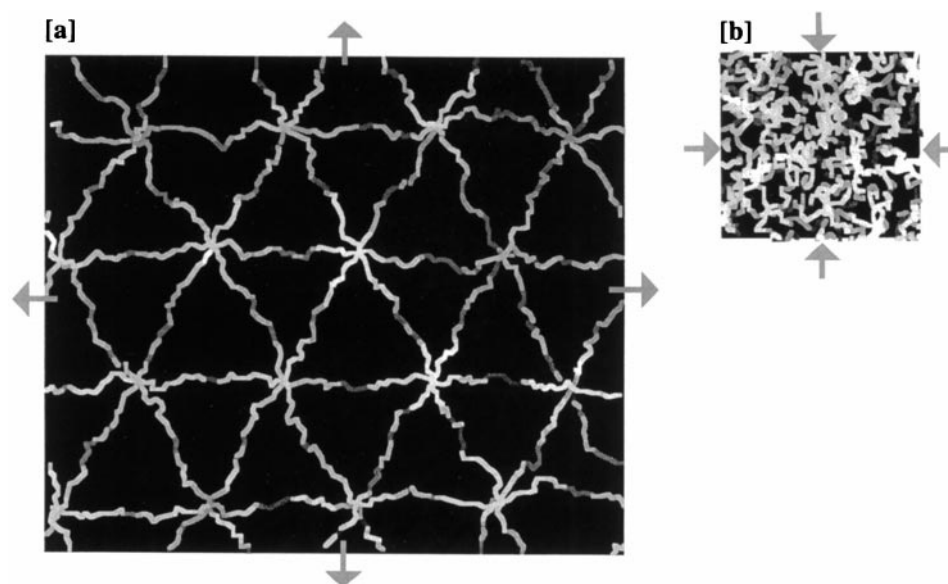


FIGURE 1 Periodic box configurations of a model cytoskeleton at $\beta\Pi a^2 = -0.2$ (*a*, tension) and $\beta\Pi a^2 = 0.2$ (*b*, compression), where Π is the imposed two-dimensional stress and a is the bead diameter appearing in Eqs. 1 and 5. The chains are drawn such that elements closer to the viewer have lighter shading. The two configurations are drawn to the same scale. Simulation is from the stress-free model described in the text.

2. There may be attractive interactions between nonneighboring elements of the spectrin tetramers of the cytoskeleton (see, for example, Stokke et al., 1986; Ursitti and Wade, 1993).

We refer to our representations of situations 1 and 2 as the prestress model and condensed model, respectively. Results from all three simulations are presented and compared in this paper. Furthermore, the anisotropic response of the polymer-chain networks at moderate deformation is reported and seen to be similar to that found for two-dimensional triangulated networks (Discher et al., 1997).

The content of the paper is organized as follows. The notation and simulation techniques are reviewed in the next section. The simulation results from all three cytoskeleton models are then presented and compared, with an emphasis on the geometrical and elastic characteristics of the model cytoskeleton in the bilayer plane. These characteristics are interpreted using mean-field approaches. Some aspects of the experimental techniques for determining the elastic properties of networks also are investigated, particularly the usage of fluctuations and numerical derivatives for obtaining the elastic moduli. The paper concludes with a summary of our findings.

SIMULATION TECHNIQUES AND ANALYSIS

The ingredients of our cytoskeleton simulation model have been described in previous publications on the properties of networks at zero stress (Boal, 1994; Boal and Boey, 1995). In the model, each spectrin tetramer is represented by a single chain that has n_{seg} freely jointed segments defined by $n_{\text{seg}} + 1$ vertices. The ends of the chains are joined at sixfold coordinated junction vertices to form a network. The chain midpoints are restricted to lie in the computational xy plane, which represents a tensed or locally flat lipid bilayer in the model, but all other chain elements can undergo motions in the positive z direction. An attractive interaction between a defined set of nearest-neighbor vertices provides the chain with its linear topology, and a repulsive interaction between all vertices prevents chain segments from overlapping.

A Monte Carlo algorithm is used to propagate a computational membrane with the form of a periodic rectangle having lengths L_x and L_y in the x and y directions, respectively. The basic intervertex potential $V(r)$ of our polymer chain networks has a bead-and-tether form with two components,

$$V(r) = V_{\text{rep}}(r) + V_{\text{nn}}(r), \quad (1a)$$

where the short-range repulsive term is

$$\begin{aligned} V_{\text{rep}}(r) &= \infty & \text{for } 0 < r < a, \\ &= 0 & \text{for } r > a, \end{aligned} \quad (1b)$$

and the nearest-neighbor tethering potential is

$$\begin{aligned} V_{\text{nn}}(r) &= \infty & \text{for } 0 < r < a \text{ and } r > \sqrt{1.9}a, \\ &= 0 & \text{for } a < r < \sqrt{1.9}a. \end{aligned} \quad (1c)$$

The repulsive term applies to all vertex pairs, and the tethering potential applies only to nearest-neighbor vertices along the chain. The length scale of the system is set by the bead diameter a ; the relationship between a and the physical length scale depends upon the model, as discussed later in this section. In the limit of very small Monte Carlo step sizes, self-avoidance of the chain only requires the maximum tether length to be $\sqrt{2}a$, rather than $\sqrt{1.9}a$. However, the nonzero step size of this simulation allows chains to cross each other at $\sqrt{2}a$, and hence a slightly smaller tether length is used in Eq. 1c.

The simulation generates a set of configurations that samples periodic box shapes according to the usual ΠA -type Boltzmann weight and is used to construct ensemble averages of geometrical observables, such as the box lengths $\langle L_x \rangle$ and $\langle L_y \rangle$ or the box area $\langle A \rangle$. The elastic constants of the network can be determined from these ensemble averages, either through numerical derivatives such as

$$K_A^{-1} = \langle A \rangle^{-1} (\partial \langle A \rangle / \partial \Pi), \quad (2)$$

or via fluctuations

$$\beta K_A = \langle A \rangle / (\langle A^2 \rangle - \langle A \rangle^2), \quad (3)$$

where K_A is the in-plane area compression modulus, β is the inverse temperature $(k_B T)^{-1}$, and Π is the in-plane pressure. The in-plane shear modulus μ is obtained subsequently from

$$(\beta K_A)^{-1} - (\beta \mu)^{-1} = 4 \langle A \rangle (\langle L_x L_y \rangle / \langle L_x \rangle \langle L_y \rangle - 1). \quad (4)$$

We have checked the numerical accuracy of the calculations by comparing the results from Eqs. 2 and 3 for selected parameter values. Analogous to Eq. 3, the volume compression modulus K_V can be obtained from $\beta K_V = \langle V \rangle / (\langle V^2 \rangle - \langle V \rangle^2)$, where $V = A(z)$ and z is the distance above the bilayer plane at $z = 0$. The transverse Young's modulus Y_{tr} can be extracted from the fluctuations in z via $\beta Y_{\text{tr}} = [\langle z \rangle / (\langle z^2 \rangle - \langle z \rangle^2)] / \langle A \rangle$ (Boal and Boey, 1995).

In a previous paper (Boal and Boey, 1995), a mixed Monte Carlo/molecular dynamics algorithm was used to propagate a polymer network whose interactions were smooth functions of interparticle separation (see Bishop et al., 1979). The ensemble averages of all in-plane and almost all out-of-plane quantities calculated by this MC/MD technique are correct, and agree with pure MC simulations of the same potentials. However, the ensemble average $\langle z^2 \rangle$ is not consistent within this mixed ensemble, and hence we use only pure MC in this paper. The results of Boal and Boey (1995) on the barrier-free paths of directed protein motion are unaffected by this inconsistency in $\langle z^2 \rangle$.

The connectivity of our network junctions is strictly sixfold. However, it is claimed from electron microscopy that erythrocytes also contain junctions with five or fewer spectrin tetramers attached (Byers and Branton, 1985; Ursitti and Wade, 1993). The properties of defective networks have been investigated in statistical mechanics, and the elastic properties of one category of defective two-dimen-

sional networks at zero temperature and zero stress were determined by Hansen et al. (1996). For networks whose junction vertices have a mean connectivity near 6, the variation of the elastic moduli with the amount of defective connectivity is not a strong effect compared to the stress dependence of interest in this paper. Of course, bond-depleted networks, which are present in erythrocytes of individuals with certain hereditary blood diseases, may have much lower elastic moduli for bond concentrations approaching the rigidity percolation threshold (Thorpe, 1986; Tang and Thorpe, 1988; Saxton, 1990; Hansen et al., 1997).

In our previous two papers on polymer chain networks, we determined the behavior of a particular model network at zero stress as a general function of n_{seg} . Here we investigate the properties of three model networks as a function of in-plane compression and tension for a value of n_{seg} specific to each model. In all three situations, the parameters for the cytoskeleton model are chosen such that the contour area per junction vertex, A_c , is approximately seven times the equilibrium area per junction, $\langle A_j \rangle$. For the potential in Eqs. 1a–1c, the contour area per junction is $A_c = (\sqrt{3}/2) \times (1.2an_{\text{seg}})^2$.

Stress-free model

In this simple model, the interactions among chain elements are described strictly by Eq. 1, and the in vivo state of the erythrocyte is assumed to be stress-free. To satisfy $A_c/\langle A_j \rangle = 7$, the number of segments per polymer chain must be $n_{\text{seg}} = 26$ (see Boal, 1994). For a 200-nm contour length, the bead diameter in the model, a_{sf} , must have a physical value of 6.4 nm.

Prestress model

The ratio $A_c/\langle A_j \rangle$ increases with n_{seg} (Boal, 1994). It is possible to have $A_c/\langle A_j \rangle \approx 7$ for $n_{\text{seg}} < 26$, but the model cytoskeleton must then be in a condensed or prestressed state. Introducing the prestress $\beta\Pi_{\text{ps}}a^2$ as a new parameter, there is a locus of values for n_{seg} and $\beta\Pi_{\text{ps}}a^2$ that satisfy $A_c/\langle A_j \rangle = 7$. The polymer chain model will have difficulty in reproducing the observed elastic moduli if n_{seg} is much less than 12, so we choose $n_{\text{seg}} = 12$ as a limiting case. The assignment for the bead diameter a_{ps} of 13.9 nm with $n_{\text{seg}} = 12$ corresponds to a 200-nm contour length in the prestress model.

Condensed model

An alternative means of forcing $A_c/\langle A_j \rangle = 7$ for $n_{\text{seg}} < 26$ is to preserve the in vivo state as stress-free, but to add attractive interactions between nonneighboring vertices. We choose the attractive interaction to have a square-well form,

$$V_{\text{att}}(r) = \begin{cases} \infty & \text{for } 0 < r < a, \\ -\gamma & \text{for } a < r \leq \sqrt{1.9}a, \\ 0 & \text{for } r > \sqrt{1.9}a, \end{cases} \quad (5)$$

where the energy scale γ is chosen to satisfy $A_c/\langle A_j \rangle = 7$ for a given n_{seg} . For ease of comparison with the prestress model, we choose $n_{\text{seg}} = 12$. The variation of $A_c/\langle A_j \rangle$ with $\beta\gamma$ is shown in Fig. 2, from which one can see that $A_c/\langle A_j \rangle = 7$ is reached at $\beta\gamma = 0.6$. As in the prestress model, a 200-nm contour length corresponds to a bead diameter a_c of 13.9 nm if the chain has 12 segments.

The number of junction vertices N_j in the cytoskeleton simulations is 16, so that the total number of particles in the computational system is 544 for $n_{\text{seg}} = 12$ and 1216 for $n_{\text{seg}} = 26$. At each pressure, the sample sets consist of 1050 configurations separated by 10^4 MC steps ($n_{\text{seg}} = 12$) or 750 configurations separated by 3×10^4 MC steps ($n_{\text{seg}} = 26$), to ensure statistical accuracy of the ensemble averages. The first 50 configurations of the sample are discarded in constructing the averages. Other calculational details can be found in Boal (1994).

CYTOSKELETON SIMULATIONS

In human erythrocytes, the contour length of the spectrin tetramers is ~ 200 nm, compared to the average end-to-end distance of ~ 75 nm in vivo, meaning that the cytoskeleton can be stretched to about seven times its equilibrium area. Within the polymer-chain model, this factor of seven in the ratio of contour area per junction complex, A_c , to equilibrium area per junction, $\langle A_j \rangle$, arises from the entropic properties of the chains. That is, “slack” in spectrin fluctuates into the cytoplasm, defining an average height, analogous to a brush thickness, that should somehow correlate with the in-plane stress response of the cytoskeleton. The in-plane stress response of the stress-free model (see previous section) is illustrated in Fig. 1, which shows two configurations drawn from simulations at $\beta\Pi\sigma^2 = 0.2$ (compression) and $\beta\Pi\sigma^2 = -0.2$ (tension). The two parts of the figure are drawn to the same scale, and the difference in the network density is obvious: at $\beta\Pi\sigma^2 = 0.2$ the network is almost eight times as dense as it is at $\beta\Pi\sigma^2 = -0.2$.

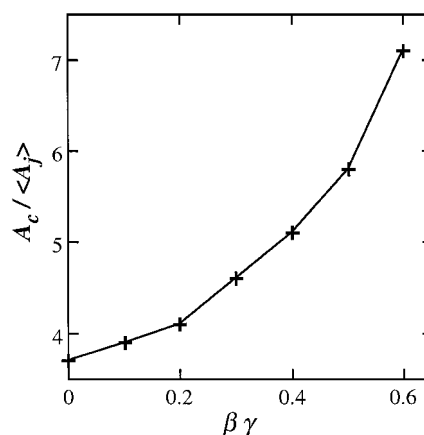


FIGURE 2 Ratio of contour area per junction A_c to average area per junction $\langle A_j \rangle$ for the condensed model, shown as a function of the energy scale $\beta\gamma$ in the attractive potential of Eq. 5.

The area per junction vertex $\langle A_j \rangle / N_j$ under both compression and tension is shown in Fig. 3 *a* for all three models. For comparative purposes, the areas are compared to the contour area per vertex A_c . Recent micropipette aspiration experiments on intact red cell membranes (Discher et al., 1994) have shown that the area (which is the inverse of the surface density reported in the paper) of the red cell network in reversible deformation can, at the least, range between 0.5 and 4 times the unstressed area, depending on the magnitude of aspiration. The results in Fig. 3 cover much of this range, and extend to even lower density (high area), where sensitivity becomes an issue in experiment.

There are several distinctive features to Fig. 3 *a*. Under increasing compression, $\langle A_j \rangle$ decreases and should ultimately tend toward a constant, determined by the steric interaction of the cytoskeleton elements. However, the small value of $\langle A_j \rangle$ at $\beta \Pi a^2 = 1.0$ is not near the close-packed density of the spherical beads, reflecting the fluctuations in position of these chain elements at finite temperature. Under tension at $-\beta \Pi a^2 > 0.5$, the area per junction approaches the contour area per junction of the network, indicated by $\langle A_j \rangle / A_c \rightarrow 1$. Both the prestress and condensed models have $n_{\text{seg}} = 12$, and they approach the contour area together. The stress-free model has $n_{\text{seg}} = 26$, a very flex-

ible network that expands more rapidly under tension than the $n_{\text{seg}} = 12$ networks do, for a given bead diameter a . Note, however, that the physical value of a is model-dependent, an issue to which we return in Fig. 8.

Both the stress-free and condensed networks have parameters (n_{seg} and $\beta \gamma$) that are selected to reproduce $\langle A_j \rangle / A_c = 1/7$. Thus both of these models have the same area per junction at $\beta \Pi a^2 = 0$. In contrast, the $n_{\text{seg}} = 12$ network without an attractive interaction (prestress model) has $\langle A_j \rangle / A_c \approx 2/7$ at $\beta \Pi a^2 = 0$, and this network must be placed under a 50% area compression with $\beta \Pi_{\text{ps}} a^2 = 0.7$ to match the experimentally measured $\langle A_j \rangle / A_c = 1/7$.

Last, as a technical issue, note that $\langle A_j \rangle / A_c$ can exceed 1 with any “soft” interaction potential such as Eq. 1, or harmonic potentials, or some of the smooth potentials common in polymer studies (e.g., Bishop et al., 1979). The contour length of a single chain in our model at any temperature is $1.2 n_{\text{seg}} a$, which is less than the fully stretched length of $1.38 n_{\text{seg}} a$. Thus, in the limit of infinite tension, $\langle A_j \rangle / A_c$ can be as large as 1.32 for Eq. 1. Unless the chain segments are forced to be rigid rods with a fixed length, then the average segment length will slowly increase as the network becomes highly stretched. Fortunately, the network deformations in which we are interested do not significantly enter this deformation regime.

The mean displacement of the network normal to the bilayer plane is shown as a function of pressure in Fig. 3 *b*. The mean displacement is the ensemble average of the displacement z over all vertices in all configurations. Simulations show that the mean thickness of the network is $\sim 2\langle z \rangle$, suggesting that monomers are restrained by their interactions so as to be relatively uniform in their distribution above the reflecting plane at $z = 0$. As expected, the trends in $\langle z \rangle$ are the reverse of those of the area: $\langle z \rangle$ is largest under compression, and decreases monotonically with increasing tension. The two networks with $n_{\text{seg}} = 12$ have very similar values for $\langle z \rangle$, despite their differences in area. Although the $n_{\text{seg}} = 26$ network has a significantly larger $\langle z \rangle$ under a compressive stress, in terms of the a length scale, its value in physical units is similar to the $n_{\text{seg}} = 12$ networks, once one takes into account that $a_{\text{ps}} = a_c \approx 2a_{\text{sf}}$. A measure of the cytoskeleton volume can be obtained from the product of the area per junction vertex from Fig. 3 *a* with the mean displacement from Fig. 3 *b*. It is important that one finds that the volume per junction is larger when the network is under tension than when it is under compression. Thus these cytoskeletal networks are far from incompressible—volumetric incompressibility being a common finding in large deformation rubber elasticity.

The in-plane compression and shear moduli are extracted from the simulations via fluctuations. The behavior of the moduli is shown in Fig. 4 for all three simulation models. The compression modulus K_A has a minimum near zero stress for all of the models, and is significantly larger at moderate deformation, whether stretched or compressed. This is expected, given the steric interactions that become increasingly important when the network is compressed,

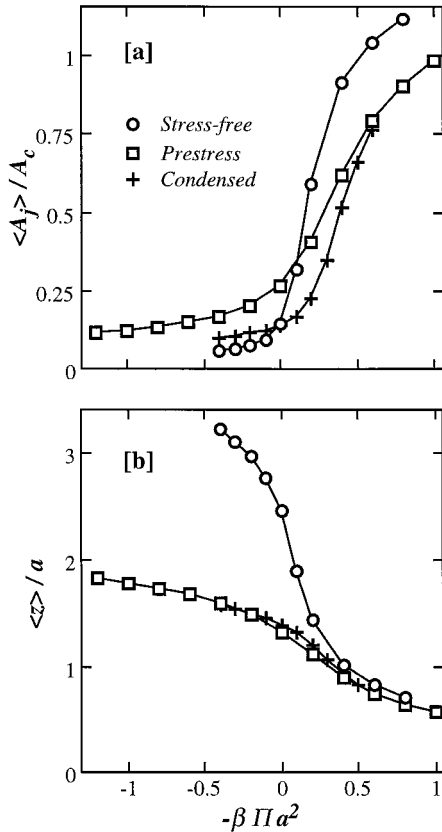


FIGURE 3 Reduced network area per junction complex $\langle A_j \rangle / A_c$ (a) and mean displacement $\langle z \rangle / a$ (b) as a function of in-plane pressure $\beta \Pi a^2$ for the three simulation models. Note that the physical value of a is model-dependent.

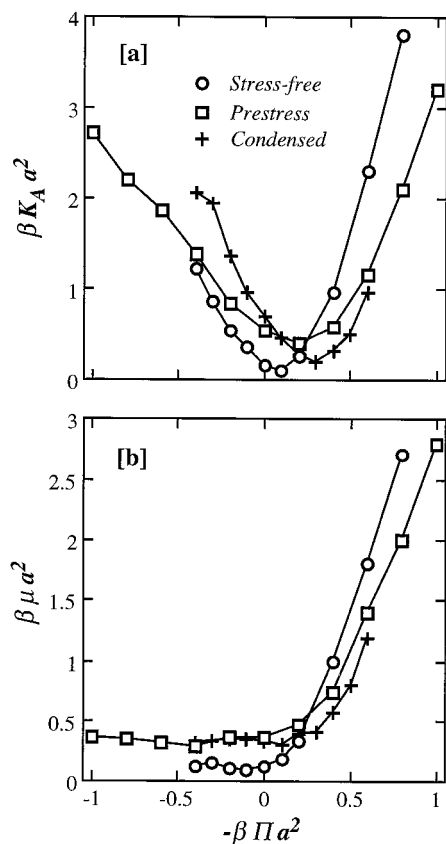


FIGURE 4 In-plane compression modulus $\beta K_A a^2$ (a) and shear modulus $\beta \mu a^2$ (b) as a function of pressure $\beta \Pi a^2$ for the three simulation models.

and given the tether constraints that resist the network being stretched much beyond $\langle A_j \rangle / A_c = 1$. Of the three networks shown in Fig. 4 a, the 26-segment network is expected to be the softest, and one can see that its compression modulus is the lowest near zero stress and under compression.

The shear modulus, shown in Fig. 4 b, shares several characteristics with the compression modulus. At large extension, the networks resist shear because of the tethering constraints, as with K_A . However, when the networks are compressed, the increased steric interaction does not cause an increase in the shear modulus, unlike the situation with K_A . However, this behavior is not unexpected, because the tethering constraints that resist shear are most important when the network is stretched, not when it is compressed, as can be seen from Fig. 1. Finally, the 26-segment network tends to have the lowest shear modulus of the three networks under compression, again as with K_A .

Two elastic moduli that depend upon the out-of-plane properties of the network are shown in Fig. 5. Generally speaking, the volume compression modulus K_V displayed in Fig. 5 a decreases slowly with stress. This behavior is similar, but not identical, to that of K_A : steric interactions will raise the compression modulus as the network is compressed. Similar behavior is seen in Fig. 5 b for the transverse Young's modulus Y_{tr} as a function of stress. As pointed out previously (Boal, 1994), one expects K_V to be

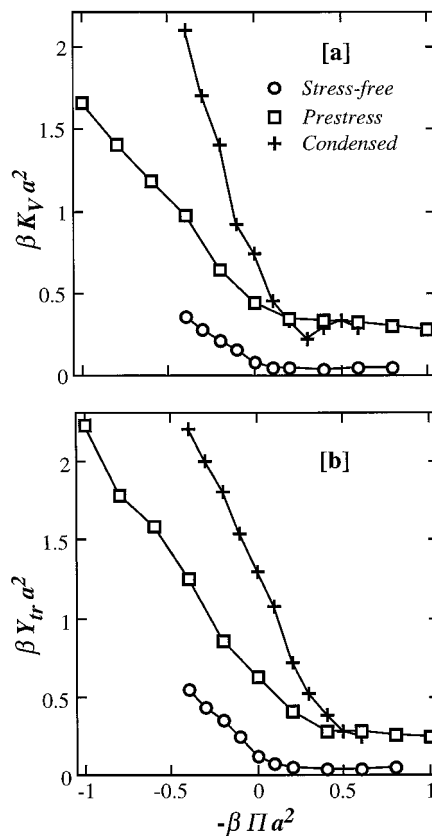


FIGURE 5 Volume compression modulus $\beta K_V a^3$ (a) and transverse Young's modulus $\beta Y_{tr} a^2$ (b) as a function of pressure $\beta \Pi a^2$ for the three simulation models.

on the order of Y_{tr} , and this rough numerical equivalency can be seen by comparing Fig. 5, a and b.

DISCUSSION

Our first task in interpreting the results from Figs. 3–5 is to develop an intuitive description of the network's in-plane behavior. The chain elements shown in Fig. 1 assume a variety of configurations: they are mildly or even excessively contorted in 3-D. However, the motion of the sixfold junctions is much more restricted, and the displacement from their mean position is fairly small relative to the interjunction separation. Thus the effective temperature of the junctions is, in a sense, much lower than the effective temperature of the chain elements, as measured by the dispersion in their positions. At moderate deformations, the junctions behave like a low-temperature network in two dimensions.

To quantify this observation, consider a network of springs, each governed by Hooke's Law:

$$V_{HL}(s) = (1/2)k_{HL}(s - s_0)^2, \quad (6)$$

where k_{HL} is the spring constant and s is the length of the spring, whose unstretched length is s_0 . At zero temperature,

a triangular network of identical springs under stress is described by (Boal et al., 1993)

$$\langle A \rangle / \langle A \rangle_0 = (1 + \Pi / \sqrt{3k_{HL}})^{-2} \quad (7a)$$

$$K_A / k_{HL} = \sqrt{3}(1 + \Pi / \sqrt{3k_{HL}}) / 2 \quad (7b)$$

$$\mu / k_{HL} = \sqrt{3}(1 - \sqrt{3}\Pi / k_{HL}) / 4, \quad (7c)$$

where $A_0 = \sqrt{3}s_0^2/2$. As in the previous section, the applied pressure Π is defined to be negative for a network under tension. According to Eqs. 7a–7c, as Π becomes more negative,

- the area increases,
- K_A decreases, and
- μ increases.

Equations 7a–7c for fixed Π provide an apt description of the spring network in the small fluctuation limit, which corresponds to $\beta k_{HL}s_0^2 \gg 1$. Furthermore, Eqs. 7b and 7c show that there is a domain of $\Pi < 0$ at which μ exceeds K_A , which implies that the Poisson ratio is negative (in two dimensions). However, Eqs. 7a–7c, for zero temperature, do not faithfully describe a spring network under moderate compression: just above $\Pi = (\sqrt{3}/8)k_{HL}$ there is a symmetry-breaking transition as the network area goes to zero discontinuously from $(8/9)^2 A_0$ (Discher et al., 1997; Wintz et al., 1997). Are any of these properties of Hookean spring networks present in the model cytoskeletons?

Harmonic regime

Inspection of the ratio of K_A/μ , shown in Fig. 6, confirms that several properties of the low-temperature spring network are present in the model cytoskeletons. The figure shows that $K_A/\mu \approx 2$ for all models at zero stress, as predicted by Eqs. 7b and 7c. Also near zero stress, K_A/μ increases under compression, again as expected from Eqs. 7b and 7c. Furthermore, there is a range of extension for

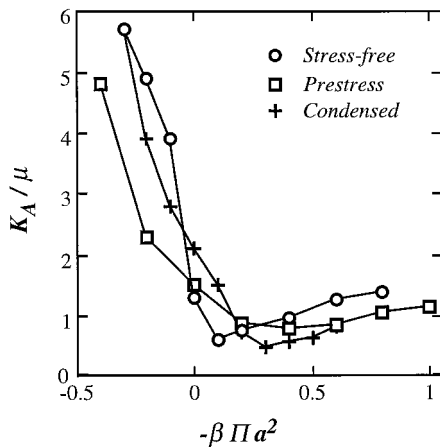


FIGURE 6 Ratio of in-plane compression modulus K_A to shear modulus μ as a function of pressure $\beta \Pi a^2$ for the three simulation models.

which $K_A/\mu < 1$, implying that the Poisson ratio is negative. With the exception of the blow-up in network area predicted by Eq. 7a at $\Pi = -\sqrt{3}k_{HL}$, but prevented in the model networks by the tether constraints, several of the generic features of a low-temperature Hooke's Law network are present in our three models at modest stress.

If the model cytoskeletons are approximately described near zero stress by Eqs. 7a–7c, then an effective spring constant k_{eff} can be determined for each model. We consider the harmonic behavior of the stress-free model in some detail, and then simply quote results for the other models. The in-plane area compression modulus $\beta K_A a^2$ of the stress-free model is observed to be 0.16 at $\Pi = 0$. Comparing this value with Eq. 7b, each chain in the network is equivalent to a spring with effective spring constant $\beta k_{\text{eff}} a^2 = 0.18$. A similar treatment of the shear modulus using Eq. 7c yields an effective spring constant of $\beta k_{\text{eff}} a^2 = 0.28$, for an average from both moduli of $\beta k_{\text{eff}} a^2 = 0.23$.

The harmonic behavior of the cytoskeleton at small stress can be confirmed from the behavior of the area as a function of stress. We plot in Fig. 7 the area per junction vertex $\langle A \rangle / N_j$ normalized to the zero stress value, which is $\langle A_j \rangle_0 = 119a^2$. At small deformations, the area follows the low temperature behavior of Eq. 7a, namely that $\langle A \rangle^{-1/2}$ is a linear function of the tension. By fitting Eq. 7a to the area around $\Pi = 0$, one finds that the effective spring constant is then $\beta k_{\text{eff}} a^2 = 0.22$, which is in very good agreement with the value extracted above from the elastic moduli. Now the area per junction at zero stress of $119a^2$ corresponds to an effective interjunction length of s_0 of $11.7a$ in the stress-free model. Expressed in terms of spring variables, the effective spring constant of the stress-free model in the harmonic regime is $\beta k_{\text{eff}} s_0^2 = 30$. This is a large spring constant corresponding to a stiff (or, equivalently, cold) network that has small fluctuations in the intervertex separation.

A similar analysis of the other two model networks yields values of $\beta k_{\text{eff}} a^2 = 0.72$ for the prestress model, and $\beta k_{\text{eff}} a^2 = 0.81$ for the condensed model, both evaluated at zero stress.

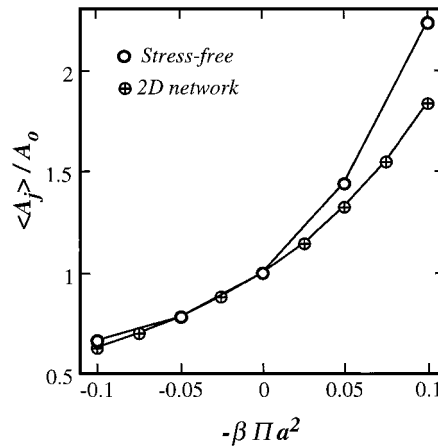


FIGURE 7 Normalized area $\langle A_j \rangle / \langle A_j \rangle_0$ as a function of pressure $\beta \Pi a^2$ for the stress-free model. A fit to the data using Eq. 7a is shown for comparison, with $\beta k_{\text{eff}} a^2 = 0.22$.

Using the average interjunction separation at zero stress as a length scale, rather than a , yields $\beta k_{\text{eff}} s_o^2 = 39$ and 23 for the prestress and condensed models, respectively. Thus we see that for small deformations, the junctions in all three models effectively behave like two-dimensional networks of springs at very low temperature.

Physical values

The areas and elastic constants are reported in dimensionless form in the simulation section of this paper. What is needed to convert these quantities to physical units are choices for the inverse temperature β and the bead diameter a . At room temperature, $\beta^{-1} = 4.0 \times 10^{-21}$ J; to mimic a 200-nm spectrin contour length, $a_{\text{sf}} = 6.4$ nm and $a_{\text{ps}} = a_c = 13.9$ nm. However, the reference configuration (i.e., the configuration assumed by the cytoskeleton of an erythrocyte in its discotic shape) is not the same in all models: the reference state is at zero stress in the stress-free and condensed models, but is under a stress $\beta \Pi_{\text{ps}} a_{\text{ps}}^2$ in the prestress model. According to Fig. 3, $\beta \Pi_{\text{ps}} a_{\text{ps}}^2$ must be equal to -0.7 to give $A_c / \langle A_j \rangle = 7$. Hence we can construct the behavior of $\langle A_j \rangle$ and the elastic moduli as a function of applied stress as long as we are careful to measure the stress with respect to the “reference” stress of the equilibrium configuration. An externally applied stress $\Delta \Pi$ is related to the stress in the model cytoskeletons by

$$\Delta \Pi = \Pi \quad (\text{stress-free and condensed models}) \quad (8a)$$

$$\begin{aligned} \beta \Delta \Pi a_{\text{ps}}^2 &= \beta \Pi a_{\text{ps}}^2 - \beta \Pi_{\text{ps}} a_{\text{ps}}^2 \\ &= \beta \Pi a_{\text{ps}}^2 + 0.7 \quad (\text{prestress model}). \end{aligned} \quad (8b)$$

The area per junction $\langle A_j \rangle$ in physical units is displayed in Fig. 8. By definition, the three models agree at $\Delta \Pi = 0$, and it is seen that the areas are very similar for $\Delta \Pi > 0$ (compression) as well. However, the networks under ten-

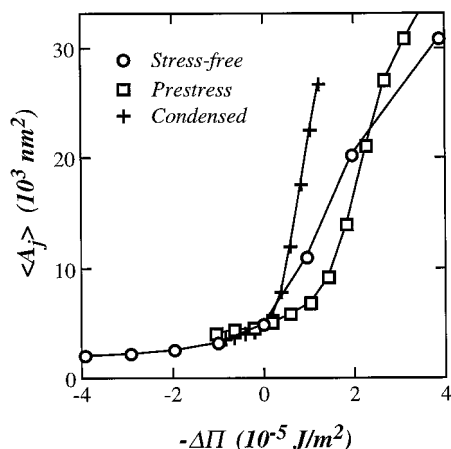


FIGURE 8 Area per junction vertex $\langle A_j \rangle$ as a function of an externally applied stress $\Delta \Pi$. Conversion to physical units is described in the text. The area is quoted in 10^3 nm^2 , and $\Delta \Pi$ is quoted in 10^{-5} J/m^2 . Note that the definition of $\Delta \Pi$ is model-dependent (see Eq. 8).

sion show quantitatively different behavior, although they share qualitative trends. At moderate tension, the area of the condensed model rises the fastest under tension, followed by the stress-free model, and trailed by the prestress model. The differences between the stress-free and prestress models are not always large, but they are significant.

The compression modulus K_A of the models, shown in Fig. 9 *a*, displays similar qualitative features: K_A is large at large values of $|\Delta \Pi|$, and has a minimum near, but not at, $\Delta \Pi = 0$. The fact that K_A has a minimum at moderate tension is expected for a harmonic network, although K_A is not observed to vanish within the cytoskeletal models, as it would in a pure Hooke's Law network, in which the spring lengths can increase without bound.

Finally, the in-plane shear modulus μ is shown in Fig. 9 *b*. At zero stress, all models display a similar value of $\sim 10^{-5} \text{ J/m}^2$, which is in the range found in the micromechanical manipulation measurements. The models also illustrate that the shear modulus has a finite value that does not change significantly when the network is placed under compression; in contrast, the shear modulus decreases and even vanishes under compression for Hooke's Law networks in two dimensions. The largest differences between the models arise when the networks are placed under tension: the shear modulus rises slowest in the prestress model.

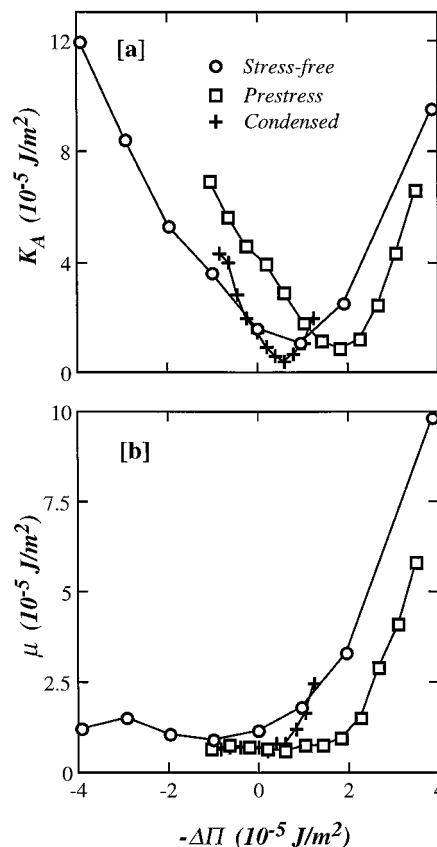


FIGURE 9 In-plane compression modulus K_A (*a*) and in-plane shear modulus μ (*b*) as a function of $\Delta \Pi$. Same conversions as in Fig. 8. All of K_A , μ , and $\Delta \Pi$ are quoted in 10^{-5} J/m^2 .

This behavior of μ is expected, given the properties of the network area under stress: the area of the prestress model increases the slowest of the three models, and so the shear-resisting tether constraints are not as important in prestress networks at modest tensions as they are in the other networks.

Anisotropic stress

The anisotropic response of two-dimensional triangulated networks at large deformations has been demonstrated for a class of Hamiltonians including simple square well interactions between nearest-neighbor network nodes (Discher et al., 1997). By “square well” potential we mean a potential that vanishes for intervertex separations s less than a fixed s_{\max} , and is infinite beyond s_{\max} (Boal et al., 1993). The stress/strain relation in one of the three tether directions is found to be different from the stress/strain relation in an orthogonal direction. However, the anisotropy only becomes marked in these nets when the strains approach 80–90% of their allowed maximum.

We have probed a model cytoskeleton for the same phenomenon of anisotropic response by applying a uniaxial stress along one of the periodic boundaries to a $n_{\text{seg}} = 12$ polymer chain network. Fig. 10 shows the strain variable $\langle L_i \rangle / \langle L_i \rangle_0 - 1$ as a function of uniaxial stress for two axes in the periodic system: $L_i = L_x$ or L_y . In the figure, the stress is applied in the same direction as the strain label, and is zero in the orthogonal direction. Young’s moduli Y_x and Y_y can be determined from the stress/strain relations presented in the figure, and compared with Y_x and Y_y extracted independently from K_A and μ (see Boal et al., 1993). Near $\Pi = 0$, the two determinations of the Young’s moduli agree to better than 10%.

One can see that there is little anisotropy in the response of the model cytoskeleton up to a 50% change in the

periodic box lengths for a given magnitude of anisotropic stress. However, the anisotropic response becomes noticeable once the strain variable exceeds ~ 0.6 . Furthermore, the stress associated with a given strain varies strongly with direction for $\langle L_i \rangle / \langle L_i \rangle_0 > 1.6$. Thus the model network responds anisotropically at large deformation, in a way similar to that observed for two-dimensional triangulated networks.

Modulus measurements at large deformation

Measurements have been made of the shear modulus of the erythrocyte cytoskeleton in two different deformation regimes. In micromechanical manipulation, the cytoskeleton is subject to at least moderate deformation, and the modulus is extracted from stress/strain relations analogous to Eq. 2. In studies of erythrocyte flicker, the modulus is found from shape fluctuations at zero stress, similar to Eq. 3. Different normalization conventions, such as the use of $\langle A \rangle_0$ rather than $\langle A \rangle$ as a normalizing area in Eq. 2, can lead to artificially different elastic constants. While one must be aware of normalization conventions when comparing results, the shear moduli determined by the manipulation and flicker techniques are different by at least an order of magnitude. Does the difference lie in the use of fluctuations rather than stress/strain relations to obtain the moduli?

Based on the fluctuation-dissipation theorem, we do not expect that Eqs. 2 and 3 should yield different moduli, although it should be emphasized that large samples are needed for Eq. 3 to yield accurate results. As a test, moduli were extracted from both relations in an analysis of the stress-free model data, covering a fourfold change in area. Over this range, the compression moduli obtained from the two approaches agreed to within 20%, entirely consistent with the uncertainty in the data. We conclude that the moduli, measured under the same conditions, should be independent of whether they are determined from fluctuations or the stress/strain relations. The difference in the two measurement techniques must arise from another source.

SUMMARY

We report simulations of the human erythrocyte cytoskeleton, using three structural models for networks tacked to a flat “bilayer”:

The *stress-free model*, in which each spectrin tetramer of the cytoskeleton is treated as a 26-segment polymer, and the elastic properties of the network arise from the entropic properties of the polymer. For this model to apply, the cytoskeleton is assumed to be stress-free in vivo.

The *prestress model*, in which there are only 12 segments per spectrin, but the network is under an externally generated prestress. This situation could arise if the membrane area decreases with cell age, without a corresponding loss of cytoskeletal material.

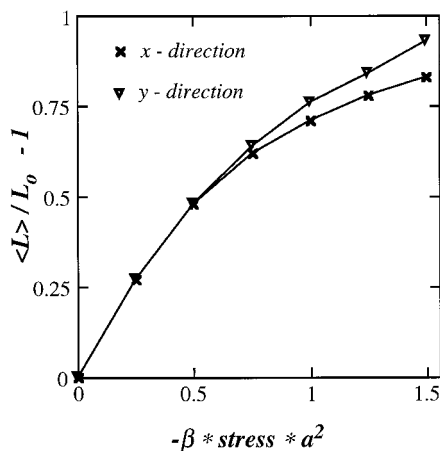


FIGURE 10 Strain variable $\langle L_i \rangle / \langle L_i \rangle_0 - 1$ as a function of uniaxial stress for two axes in the periodic system: $L_i = L_x$ and L_y . The stress is applied in the same direction as the strain label, and is zero in the orthogonal direction.

The *condensed model*, in which there are 12 segments per spectrin, and an attractive interaction between nonneighboring spectrin elements within a given chain and between different chains.

In each of these models, the reference area of the network is \sim one-seventh of the contour area. The properties of the networks are determined under large deformations of up to a fourfold change in equilibrium area.

The qualitative behaviors of the three models are similar:

The network area increases under tension and decreases under compression, but does not show the area collapse observed for two-dimensional triangulated networks under compression.

The network height is a quantity that fluctuates about a mean, but it invariably decreases under tension and increases under tension.

The area compression modulus increases at large deformation under both compression and tension.

The shear modulus increases under tension, but is relatively unchanged under compression.

The above behavior of the elastic moduli is expected from the nature of the constraints on the network: the dominant effects under tension arise from the chains reaching their maximum extension, whereas the dominant effects under compression are steric in origin, and have no strong influence on the shear modulus.

Although the chains themselves have considerable configurational freedom, the sixfold junctions of the chains show much more restricted motion. The junctions behave like a low-temperature triangulated network of springs, with an effective spring constant $\beta k_{\text{eff}} s_o^2$ of 20–40, depending on the model, where s_o is the equilibrium separation between junctions. The elastic moduli and the pressure dependence of the area per junction yield consistent results for the effective spring constant. Although a comparison with networks of Hookean springs proves useful in the neighborhood of zero stress, such distinguishing model features as a constant shear modulus under network compression and a limiting contour area appear to be captured more effectively by balancing worm-like chain elasticity (Marko and Siggia, 1995) against bead sterics as shown in paper II (Discher et al., 1998).

The models vary in detail when their results are converted from simulation units to physical units. Of the three, the network of the condensed model tends to be the most extensible, and shows the most rapid increase in area when the network is placed under tension. The prestress model is the least extensible, at least for moderate tension. All models show similar values for the shear modulus near zero stress. That the computed shear modulus approximates the modulus determined originally from micromechanical experiments (Waugh and Evans, 1979) is somewhat fortuitous, in that the experiments were tacitly analyzed under the assumption that the network's K_A is infinite, rather than a quantity of order μ .

One polymer-chain network was tested for anisotropic response to a uniaxial stress at large deformation. The

model cytoskeleton shows a clear anisotropic response when the strain variable $\langle L_i \rangle / \langle L_i \rangle_o - 1$ exceeds ~ 1 (where $L_i = L_x$ or L_y), although the anisotropy is very small as this strain variable approaches zero. It is important that although the anisotropy of another spectrin-actin based membrane skeleton, that of the auditory outer hair cell, is experimentally well documented (Tolomeo et al., 1996, and references therein), the anisotropy presented in the red cell cytoskeleton model here is a novel and distinctive structural feature worth searching for in large deformation experiments with red cell membranes. Last, two methods have been used experimentally for extracting the elastic moduli: stress/strain relations such as those in Eq. 2, and fluctuation relations such as those in Eq. 3. Our simulations in the stress-free model demonstrate that the two approaches yield the same results within statistical error.

The authors wish to thank Evan Evans for several spirited conversations.

This work is supported in part by the Natural Sciences and Engineering Research Council of Canada, which also provided a postgraduate scholarship for SKB. DED was supported in part through a postdoctoral fellowship from the U.S. National Science Foundation. Financial and other contributions from the Canadian Institute for Advanced Research, as well as Simon Fraser University, are very gratefully acknowledged.

REFERENCES

- Aronovitz, J., and T. Lubensky. 1988. Fluctuations of solid membranes. *Phys. Rev. Lett.* 60:2634–2637.
- Bishop, M., M. H. Kalos, and H. L. Frisch. 1979. Molecular dynamics of polymeric systems. *J. Chem. Phys.* 70:1299–1304.
- Boal, D. H. 1994. Computer simulation of a model network for the erythrocyte cytoskeleton. *Biophys. J.* 67:521–529.
- Boal, D. H., and S. K. Boey. 1995. Barrier-free paths of directed protein motion in the erythrocyte plasma membrane. *Biophys. J.* 69:372–379.
- Boal, D. H., U. Seifert, and J. C. Shillcock. 1993. Negative Poisson ratio in two-dimensional networks under tension. *Phys. Rev. E* 48:4274–4283.
- Byers, T. J., and D. Branton. 1985. Visualizations of the protein associations in the erythrocyte membrane skeleton. *Proc. Natl. Acad. Sci. USA* 82:6153–6157.
- David, F., and E. Gutter. 1988. Crumpling transition in elastic membranes: renormalization group treatment. *Europhys. Lett.* 5:709–713.
- Discher, D. E., D. H. Boal, and S. K. Boey. 1997. Phase transitions and anisotropic responses of planar triangular nets under large deformation. *Phys. Rev. E* 55:4762–4772.
- Discher, D. E., D. H. Boal, and S. K. Boey. 1998. Simulations of the erythrocyte cytoskeleton at large deformation. II. Micropipette aspiration. *Biophys. J.* 75:1584–1597.
- Discher, D., N. Mohandas, and E. A. Evans. 1994. Molecular maps of red cell deformation: hidden elasticity and in situ connectivity. *Science* 266:1032–1035.
- Engelhardt, J., and E. Sackmann. 1988. On the measurement of shear elastic moduli and viscosities of erythrocyte plasma membranes by transient deformation in high frequency electric fields. *Biophys. J.* 13: 941–965.
- Goulian, M., R. Bruinsma, and P. Pincus. 1993. Long-range forces in heterogeneous fluid membranes. *Europhys. Lett.* 22:145–150.
- Hansen, J. C., R. Skalak, S. Chien, and A. Hoger. 1996. An elastic network model based on the structure of the red blood cell membrane skeleton. *Biophys. J.* 70:146–166.
- Hansen, J. C., R. Skalak, S. Chien, and A. Hoger. 1997. Influence of network topology on the elasticity of the red blood cell membrane skeleton. *Biophys. J.* 72:2369–2381.

- Hochmuth, R. M. 1987. Properties of red blood cells. In *Handbook of Bioengineering*. R. Skalak and S. Chien, editors. McGraw-Hill, New York. 12.1–12.17.
- Kozlov, M. M., and V. S. Markin. 1990. Model of red blood cell membrane skeleton. In *Contemporary Problems of Biomechanics*. G. G. Chernyi and S. A. Regirer, editors. CRC Publications, Grand Rapids, MI.
- Le Doussal, P., and L. Radzihovsky. 1992. Self-consistent theory of polymerized membranes. *Phys. Rev. Lett.* 69:1209–1212.
- Liu, S., L. Derick, and J. Palek. 1987. Visualization of the hexagonal lattice in the erythrocyte membrane skeleton. *J. Cell Biol.* 104:527–536.
- Marko, J. F., and E. D. Siggia. 1995. Stretching DNA. *Macromolecules*. 28:8759–8770.
- Mohandas, N., and E. Evans. 1994. Mechanical properties of the red cell membrane in relation to molecular structure and genetic defects. *Annu. Rev. Biophys. Biomol. Struct.* 23:787–818.
- Mohandas, N., and W. Groner. 1989. Cell membrane and volume changes during red cell development and aging. *Ann. N.Y. Acad. Sci.* 554: 217–224.
- Nelson, D. R., and L. Peliti. 1987. Fluctuations in membranes with crystalline and hexatic order. *J. Physique*. 48:1085–1092.
- Peterson, M. A., H. Strey, and E. Sackmann. 1992. Theoretical and phase contrast microscope eigenmode analysis of erythrocyte flicker: amplitudes. *J. Phys. II (France)*. 2:1273–1285.
- Saxton, M. J. 1990. The membrane skeleton of erythrocytes: a percolation model. *Biophys. J.* 57:1167–1177.
- Steck, T. L. 1989. Red cell shape. In *Cell Shape: Determinants, Regulation and Regulatory Role*. W. Stein and F. Bronner, editors. Academic Press, New York. 205–246.
- Stokke, B. T., A. Mikkelsen, and A. Elgsaeter. 1986. The human erythrocyte membrane skeleton may be an ionic gel. I. Membrane mechanical properties. *Eur. Biophys. J.* 13:203–218.
- Strey, H., M. Peterson, and E. Sackmann. 1995. Measurement of erythrocyte membrane elasticity by flicker eigenmode decomposition. *Biophys. J.* 69:478–488.
- Svoboda, K., C. F. Schmidt, D. Branton, and S. M. Block. 1992. Conformation and elasticity of the isolated red blood cell membrane skeleton. *Biophys. J.* 63:784–793.
- Tang, W., and M. Thorpe. 1988. Percolation of elastic networks under tension. *Phys. Rev.* B37:5539–5551.
- Thorpe, M. 1986. Elastic properties of network glasses. *Ann. N.Y. Acad. Sci.* 484:206–213.
- Tolomeo, J. A., C. R. Steele, and M. C. Holley. 1996. Mechanical properties of the lateral cortex of mammalian auditory outer hair cells. *Biophys. J.* 71:421–429.
- Ursitti, J. A., and J. B. Wade. 1993. Ultrastructure and immunocytochemistry of the isolated human erythrocyte membrane skeleton. *Cell Motil. Cytoskeleton*. 25:30–42.
- Waugh, R., and E. A. Evans. 1979. Thermoelasticity of red blood cell membrane. *Biophys. J.* 26:115–132.
- Wintz, W., R. Everaers, and U. Seifert. 1997. Mesh collapse in two dimensional elastic networks under compression. *J. Phys. I (France)*. 7:1097–1111.
- Zilker, A., M. Ziegler, and E. Sackmann. 1992. Spectral analysis of erythrocyte flickering in the $0.3\text{--}4\ \mu\text{m}^{-1}$ regime by microinterferometry combined with fast image processing. *Phys. Rev.* A46:7998–8001.